Supplementary material to "The upper-mantle transition zone beneath the Ibero-Maghrebian region as seen by teleseismic Pds phases", L. Bonatto, M. Schimmel, J. Gallart and J. Morales, *Tectonophysics*, doi: 10.1016/j.tecto.2015.02.002

2015

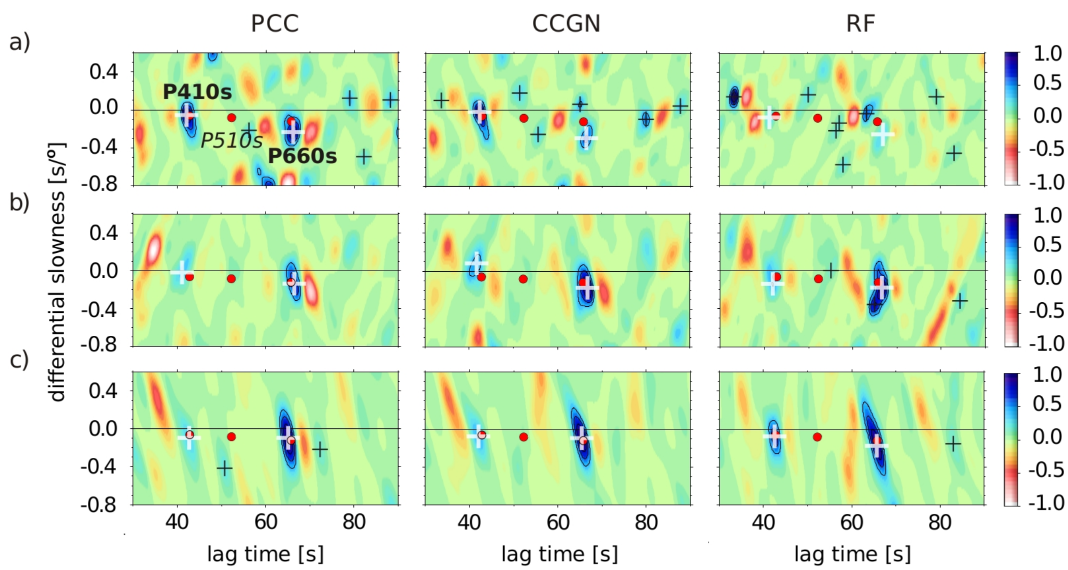

Figure S1: Representative examples of PCC, CCGN, and RF stacks that have passed the quality controls. The central latitude and longitude of the CPP-bins are: a) (37°N,0°), b) (37.75°N,1°W), and c) (42.75°N,1.5°W). Red circles mark the theoretical relative travel time and slowness values for the $P410s$, $P510s$ and $P660s$ phases. As the 510 is not a first order discontinuity in AK135, we included this discontinuity in AK135 by introducing an imperceptible increase in the density at a depth of 510 km. White crosses show detections of $P410s$ and $P660s$, while black crosses show other automatically-detected positive-amplitude maxima.

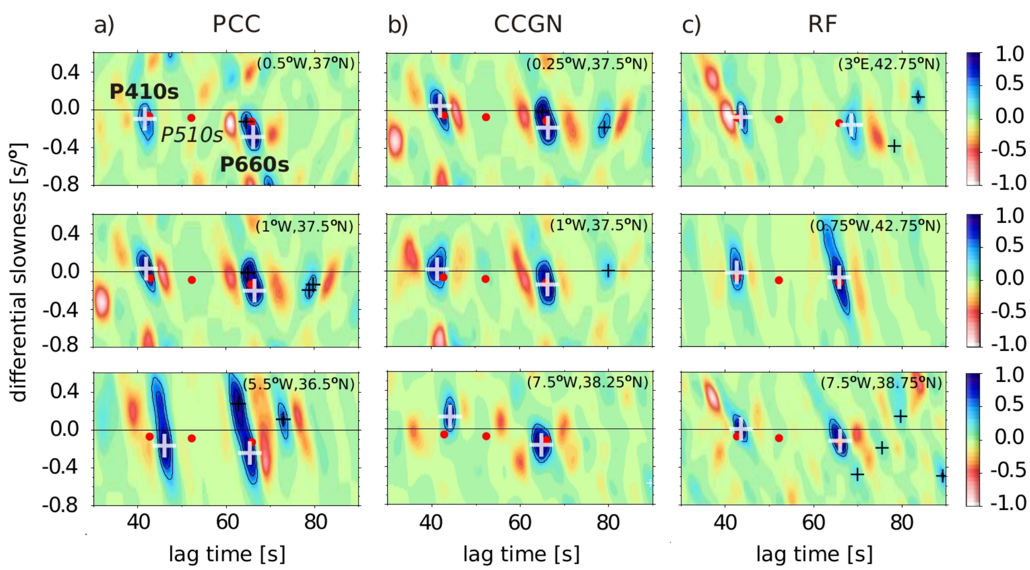

Figure S2: Selected examples of a) PCC, b) CCGN and c) RF stacks that have passed the quality controls. These examples were selected based on the clear visual detection of both phases. The central latitude and longitude of the CPP-bins are shown at the upper right corner of each stack. Red circles mark the theoretical relative travel time and slowness values for the $P410s$, $P510s$ and $P660s$ phases. White crosses show detections of $P410s$ and $P660s$, while black crosses show other automatically-detected positive-amplitude maxima.

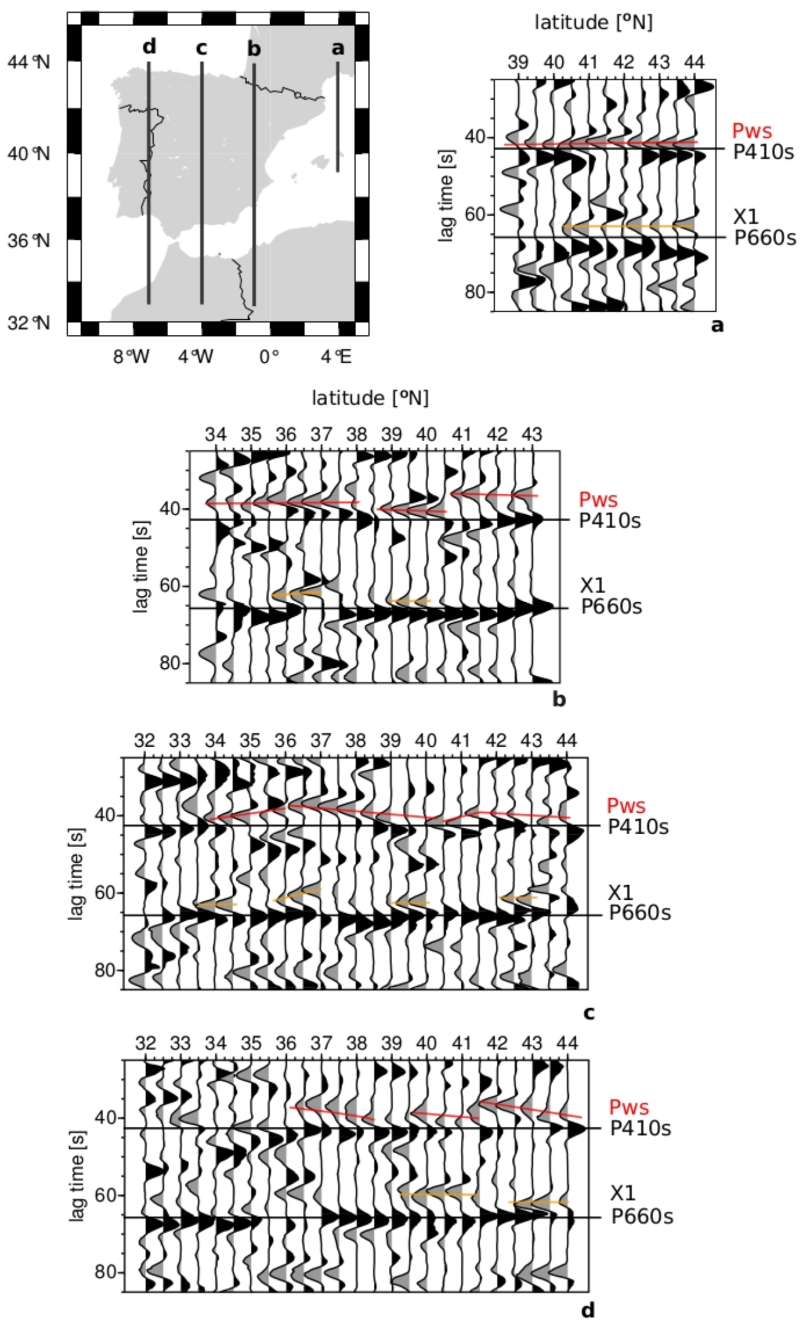
d
c
b
a
44°N
40°N
36°N
32°N
8°W
4°W
0°
4°E
latitude [°N]
lag time [s]
Pws
P410s
X1
P660s
a
b
c
d

Figure S3:

Figure S3 (*continuation*): Cross-sections of CPP-stacked RFs along fixed longitudes: a) 4°E, b) 1°W, c) 4°W and d) 7°W. The records begin 25 s after the P arrival to mask out the time interval dominated by crustal reverberations. The cross-sections show the CPP stacks in bins of 1° width in latitude and longitude and centred every 0.5°. The stacks were performed using the theoretical relative slowness of $P410s$ in AK135 ($-0.064\ s/°$). An automatic gain control (AGC with a window of 7 s) was applied to balance the amplitudes and to account for the attenuation of signals due to the use of a fixed reference slowness. The 7 s AGC window was chosen to keep the relative amplitude of contiguous signals. Solid black lines mark the reference travel time for the $P410s$ and $P660s$ phases, red lines show the arrival of negative-amplitude signals before the $P410s$, which we denoted $P\mathrm{w}s$ and orange lines mark the detection of negative-amplitude arrivals before P660s.

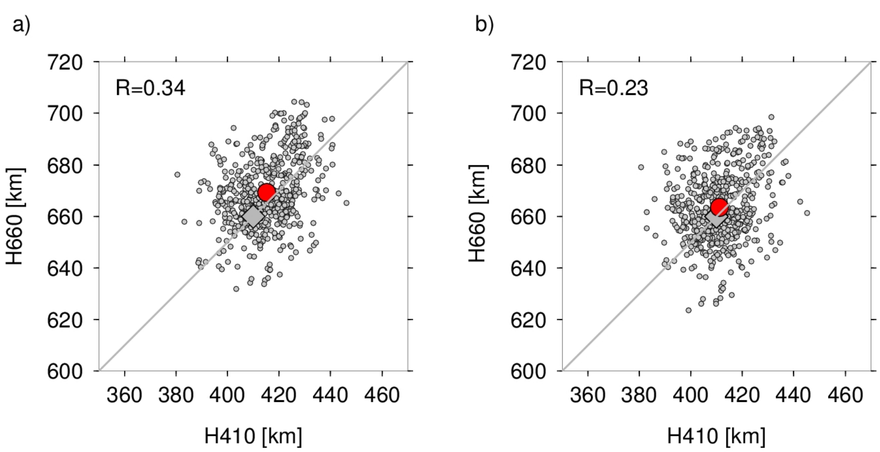

Figure S4: Relation between $H660$ and H410 obtained from a) $H660$ and $H410$ observed (before time corrections) and b) $H660$ and $H410$ observed and corrected by the tomography model of Villaseñor et al. (2003) (after time corrections). Mean value of (H410,H660) is denoted with the red circle, while grey square denotes the reference value in AK135. The grey line represents the equation $H660 = H410 + 250$ km, where 250 km is the TZT in AK135. The correlation coefficient between $H410$ and $H660$ is given at the upper left corner of each diagram.

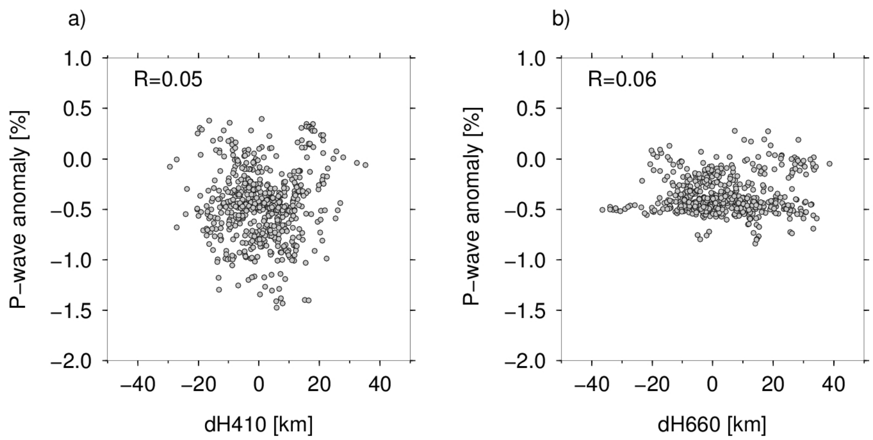

Figure S5: Average tomographic P-wave velocity anomalies in the top 400 km of the tomographic model of Villaseñor et al. (2003) versus the 410 topography dH410 (after time correction). b) Average tomographic P-wave velocity anomalies in the top 700 km versus the 660 topography dH660 (after time correction). The correlation coefficients are given at the upper left corner of each diagram; correlation coefficients before correction were a) R=-0.2 and c) R=-0.15.

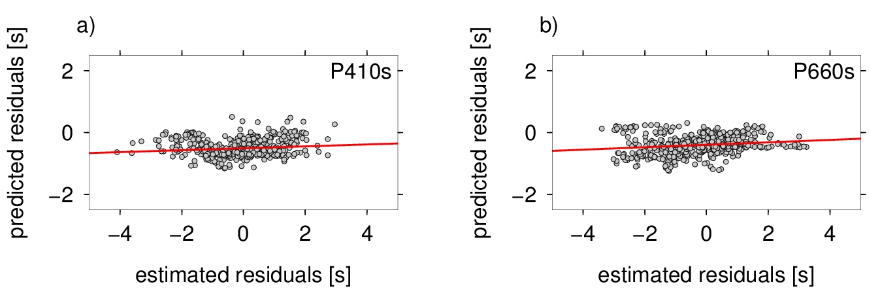

Figure S6: Comparison between predicted residuals or time corrections (defined as $tPds$, predicted by AK135 minus $tPds$ predicted by the tomography model of Villaseñor et al. (2003); $tPds_{AK135} - tPds_{tomography}$) and estimated residuals ($tPds_{AK135} - tPds_{obs,corrected}$) a) d=410 and b) d=660.